



Cite this: *RSC Adv.*, 2020, 10, 21509

Received 18th March 2020
Accepted 20th May 2020

DOI: 10.1039/d0ra02495c

rsc.li/rsc-advances

Acquiring an effective CaO-based CO₂ sorbent and achieving selective methanation of CO₂†

Chao Ping, Bao-Qi Feng, Yun-Lei Teng, * Han-Qing Chen, Si-Li Liu, Yun-Long Tai, Hao-Nan Liu and Bao-Xia Dong*

CO₂ capture, utilization, and storage are promising strategies to solving the problems of superfluous CO₂ or energy shortage. Here, mechanochemical reduction of CO₂ by a MgH₂/CaH₂ mixture was first performed, by which we achieve selective methanation of CO₂ and acquire an effective CaO-based CO₂ sorbent, simultaneously. The selectivity of methanation is near 100% and the yield of CH₄ reaches 30%. Four MgO and carbon-doped CaO-based CO₂ sorbents (MgO/CaO/C, MgO/2CaO/C, MgO/4CaO/C, and MgO/8CaO/C) were formed as solid products in these reactions. Among them, the MgO/4CaO/C sorbent shows high initial adsorption amount of 59.3 wt% and low average activity loss of 1.6% after 30 cycles. This work provides a novel, well-scalable, and sustainable approach to prepare an efficient inert additive-including CaO-based CO₂ sorbent and selectively convert CO₂ to CH₄ at the same time.

Introduction

Compared with the growth rate of anthropogenic CO₂ emissions during 1970–2000 (1.7%/year), the even growth rate of 2.6%/year during 2000–2014, is significantly increased.¹ The Intergovernmental Panel on Climate Change (IPCC) proposed that the distinct increase of the CO₂ concentration is responsible for climate change in recent years.^{2,3} Thus it is essential to considerably reduce global CO₂ emissions in the future.^{4,5} It is widely accepted that CO₂ capture, utilization, and storage are promising strategies for mitigating CO₂ emissions in short to midterm.⁶

Based on the reversible gas–solid reaction of CaO with CO₂ to produce CaCO₃, CaO-based material is considered to be a promising high-temperature solid CO₂ sorbent.⁷ CaO becomes a promising CO₂ adsorbent not only because the raw material is low costs and widely available from natural CaO precursors, *e.g.*, chicken eggshells, limestone, but also because it possesses a high theoretical CO₂ adsorption capacity of 0.78 g (CO₂) g (sorbent)^{−1}.⁴ Yet, the major problem hindering the practical application of CaO-based sorbents is the activity loss in the process of the carbonation/calcination cycles. It is generally believed that the reduced surface area, due to sintering and agglomeration of CaO particles at high temperatures, results in activity loss during the reaction cycles.⁸

At present, many procedures have been adopted to enhance the sintering-resistant property of CaO-based sorbents. There

are mainly two kinds of methods used.⁹ One is the morphology adjustment of CaO, based on particle size and microstructure. For instance, Wang *et al.* synthesized a new calcium oxide by the hydration–dehydration technology, which shows improved cycle performance.¹⁰ Broda *et al.* used a sol–gel technique to synthesize a CaO-based CO₂ sorbent that has higher surface area and larger pore volume and exhibits excellent CO₂ capture characteristics over multiple cycles.¹¹ Another method is to incorporate an inert material into the CaO. For example, Al-doped Ca–Al–CO₃ was prepared by Chang *et al.* for high-temperature CO₂ adsorption through the hydrothermal decomposition of the precursor of the coprecipitated hydroxalite.¹² In the study of Ping *et al.*, a novel Zr-doped nano-CaO adsorbent with a cage-like hollow sphere structure was prepared by ion precipitation method using carbon spheres as a template to improve the durability of CO₂ adsorption.¹³ Materials such as attapulgite,¹⁴ manganese salts,¹⁵ Zr,¹³ SiO₂,¹⁶ Y₂O₃,¹⁷ TiO₂, Al₂O₃,¹⁸ MgO, SrO,¹⁹ *et al.* were doped into CaO-based sorbents for improving CO₂ adsorption performance. Among the various available inert materials, MgO has high stability and high Tamman temperature (1400 °C).²⁰ In addition, MgO is cheaper and, therefore, most promising for improving the performance of CaO-based sorbents. Huang *et al.* developed a new and facile solvent-nonsolvent method for the preparation of MgO/CaO composites, which retain 95.3% of its initial capacity after seven cycles.²¹ Ping *et al.* prepared MgO-coated CaO-based adsorbent. They found that the thickness of the coating layer could be modified by varying MgO content, and the optimum amount of CO₂ adsorption was 36.1 wt%.²² Through these synthetic methods, effective dispersion of MgO in the CaO structure is achieved, the MgO-doped CaO-based adsorbent having a high surface area, and a favorable pore structure being

School of Chemistry and Chemical Engineering, Yangzhou University, Yangzhou, 225002, P. R. China. E-mail: ylteng@yzu.edu.cn; bxdong@yzu.edu.cn

† Electronic supplementary information (ESI) available: Pore size distributions of sorbents. See DOI: 10.1039/d0ra02495c



prepared. However, the methods in these reports often involve multiple procedures or several types of devices that are difficult to apply to the synthesis of large-scale CaO-based adsorbents. In addition, a large amount of solution is needed, which will cause secondary pollution.

In addition, CO₂ is also considered to be an inexpensive, non-toxic and abundant C1 raw material. The reduction of CO₂ to CH₄ has been extensively investigated because CH₄ is considered a promising clean fuel and can also be used as feedstock for the production of other carbon-containing chemicals.³³ Reducing CO₂ to be hydrocarbon fuels, such as CH₄ and CH₃OH, is a promising way to solve the problem of superfluous CO₂ and energy shortage.^{34,35} In this work, we achieve selective methanation of CO₂ and acquire effective CaO-based CO₂ sorbent simultaneously by reactions of CO₂ with MgH₂/CaH₂ mixture. It is a green, sustainable and scalable method to acquire effective CaO-based CO₂ sorbent.

Experimental

Mechanochemical reaction of MgH₂ and CaH₂ mixture with CO₂

MgO and carbon-doped CaO composites were synthesized by ball milling using magnesium hydride (MgH₂, 99%, Alfa Aesar), calcium hydride (CaH₂, 98%, Alfa Aesar) and CO₂ as precursors. MgH₂ and CaH₂ were weighed according to different molar ratios (with 1 : 1, 1 : 2, 1 : 4, and 1 : 8 mol mol⁻¹ ratios) and placed in a steel jar having an internal volume of 70 cm³, which contains 30 steel balls with a diameter of 6 mm. CO₂ gas (0.25 MPa) was introduced into the steel jar containing raw materials, ensuring the molar ratio of MH₂ (M = Mg and Ca)/CO₂ = 2/1.2 mol mol⁻¹. The mechanochemical reaction of MH₂ with CO₂ was carried out at 550 rpm min⁻¹ for 24 h using a planetary ball mill (QM-3SP4) at room temperature. The ball milling equipment was set to pause for 0.5 h after grinding per hour to avoid the effect of temperature rise on sample preparation during high-speed rotation of the steel ball. All sample treatments were performed in an Ar-filled glove box.

Characterization of gas and solid products in the reaction of MgH₂ and CaH₂ mixture with CO₂

Analysis of the generated gas was performed by an on-line gas chromatograph (GC) (SP-6890), using a TDX-01 column connected to a TCD detector. The gas components produced in the reaction were further analyzed by gas transmission Fourier transform infrared spectroscopy (FTIR) (Vertex 70v, Bruker, Germany) in transmission mode. The X-ray powder diffraction (XRD) patterns of the solid composites were analyzed by X-ray diffractometer (AXS D8 ADVANCE, Bruker, Germany) in the range of 10° ≤ 2θ ≤ 80° with a step size of 0.019° and a scanning rate of 0.1 s per point. To prevent being oxidized during XRD measurements, samples were covered with polyimide sheets. The BET surface area and BJH pore volume of four adsorbents were determined by N₂ adsorption measurements at -196 °C using a Micromeritics ASAP 2020 HD88 instrument. Each adsorbent was degassed at room temperature for 10 h before

measurement. The pore volume was measured at a relative pressure (P/P_0) of 0.995. The morphology of the sample was analyzed using a scanning electron microscope (SEM) (Japan S-4800II, Hitachi) at 15.0 kV, and the local elemental composition was determined by energy-dispersive X-ray spectroscopy (EDS). Materials were sputter-coated with gold for 60 s before analysis. XPS and Raman spectra were characterized by PHI 5000 VersaProbe system and DXRxi microscopy imaging spectrometers, respectively.

CO₂ carbonation and calcination

The adsorption quantity and stability of the CO₂ sorbents were examined by a synchronous thermal analyzer DSC (Differential Scanning Calorimeter)-TG (Thermo Gravimetric) (Netzsch STA 449 F3 Jupiter) with a high-sensitivity auncel (<0.1 μg). For CO₂ adsorption measurement, the sample (10–15 mg) was loaded into an alumina sample pan. A small mass was used to avoid undesired effects related to CO₂ diffusion resistance. In each test, the samples were pretreated for 15 min at 800 °C under a flow of 100% Ar (30 mL min⁻¹) to remove any physisorbed H₂O and/or CO₂ prior to the CO₂ sorption and cyclic experiments. For carbonation, the samples were heated in alumina pans from room temperature to 650 °C with a heating rate of 20 °C min⁻¹ and held for 2 h (100% CO₂, the flow rate of 50 mL min⁻¹), while the decarbonation was performed at 800 °C for 15 min (100% Ar, a flow rate of 30 mL min⁻¹). After the decarbonation treatment, the samples were again cooled to 650 °C, and the purge gas was converted from Ar to CO₂ for carbonation. The change of sample weight and temperature were continuously monitored and recorded by the instrument throughout the process. The cycle was conducted 30 times to obtain the cyclability and stability of the carbonation–calcination.

Results and discussion

Acquiring MgO and carbon-doped CaO-based CO₂ sorbent and achieving selective methanation of CO₂

Fig. 1 shows the diagram of achieving selective methanation of CO₂ and acquiring the CaO-based CO₂ sorbent by the reaction of MgH₂/CaH₂ mixture with CO₂. The gas products produced in the ball milling reactions between the MgH₂/CaH₂ mixtures (with 1 : 1, 1 : 2, 1 : 4 and 1 : 8 mol mol⁻¹) and CO₂ at 550 rpm

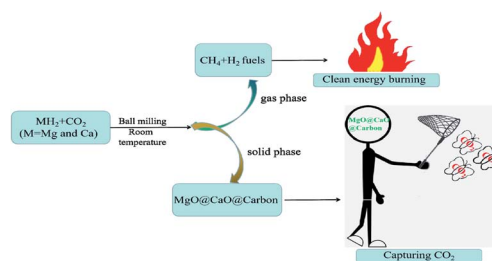


Fig. 1 Schematic diagram of achieving selective methanation of CO₂ and acquiring the CaO-based CO₂ sorbent by the reaction of MgH₂/CaH₂ mixture with CO₂.



for 24 h were characterized by GC and FTIR. It can be seen from the GC curves in Fig. 2 that there are peaks of H_2 and CH_4 , indicating that the CO_2 is methanated after the reaction and some H^{-1} in the MgH_2 is oxidized to H_2 . The FTIR spectrum of these gas products is shown in Fig. 3. Only sharp CH_4 peaks are observed, which further proves that CH_4 is formed in the reactions and implies that the reduction of CO_2 to CH_4 by the MgH_2/CaH_2 mixture is highly selective. There are no characteristic peaks of CO_2 and CO , indicating that CO_2 is wholly reduced and there is no by-product (CO) in the gas products. As shown in Table 1, for the four reactions, the conversion of CO_2 is 100% and the yield of CH_4 is 14%, 18%, 30% and 16%, respectively.

XRD pattern of the solid products for the ball milling reactions between the MgH_2/CaH_2 mixtures (with 1 : 1, 1 : 2, 1 : 4 and 1 : 8 mol mol⁻¹) and CO_2 at 550 rpm for 24 h is shown in Fig. 4. Only the characteristic peaks of CaO and MgO are observed from the XRD patterns of the solid products. There are almost no characteristic peaks of CaH_2 and MgH_2 , showing that the metal hydrides are completely consumed. As can be seen from Fig. 4a, when the molar ratio of CaH_2 to MgH_2 is 1 : 1 in the reagent, the product XRD contains characteristic peaks of CaO and MgO with almost equal intensity. It is seen from Fig. 4b–d, however, that as the molar ratio of CaH_2 in the reactant increases, the characteristic peak intensity of CaO in the product gradually increases, and the characteristic peak of MgO gradually becomes weak. This indicates that the content of CaO in the solid product gradually increases with the relative amount of CaH_2 in the reactant increasing. The broad peak at 10°–20° results from polyimide sheet, which is used to protect the samples from oxidation during XRD measurements.

XPS and Raman spectra (Fig. S2 and S3†) prove that there is amorphous carbon and a little of carbonate in the solid products formed in the reaction of alkaline earth metal hydrides with CO_2 , which is consistent with previous studies.³⁶ The solid products acquired in the reactions between the MgH_2/CaH_2 mixtures (with 1 : 1, 1 : 2, 1 : 4 and 1 : 8 mol mol⁻¹) and CO_2 are therefore named $MgO/CaO/C$, $MgO/2CaO/C$, $MgO/4CaO/C$, and

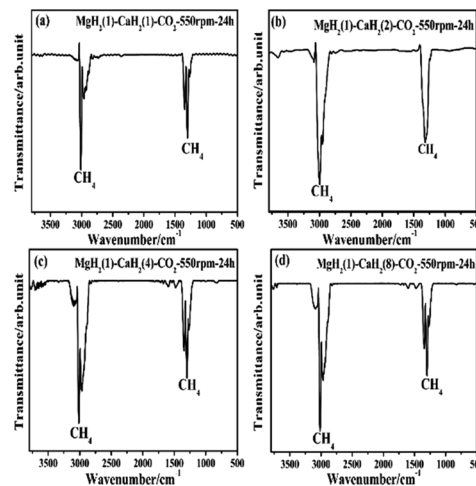


Fig. 3 FTIR spectrum of the gas products for the ball milling reactions between the MgH_2/CaH_2 mixtures (with 1 : 1, 1 : 2, 1 : 4 and 1 : 8 mol mol⁻¹) and CO_2 at 550 rpm for 24 h.

$MgO/8CaO/C$, respectively. The molar ratio of MgO to CaO in the $MgO/CaO/C$, $MgO/2CaO/C$, $MgO/4CaO/C$, and $MgO/8CaO/C$ composite is about 1 : 1, 1 : 2, 1 : 4 and 1 : 8 mol mol⁻¹, respectively. The amount of C was estimated according to the proposed reaction mechanism (eqn (S1)–(S3)†).³⁶ The molar amount of amorphous carbon in the samples ($MgO/CaO/C$, $MgO/2CaO/C$, $MgO/4CaO/C$, $MgO/8CaO/C$) is 0.007, 0.006, 0.0056 and 0.0068 mol, respectively.

The microstructure of sorbent plays key roles in the reactions of sorbent with CO_2 , and also affects on the diffusion of CO_2 over sorbent. The SEM images of the four sorbents are shown in Fig. 5, through which we can see the microscopic topography of the sorbents. With the proportion of calcium oxide increasing in the sorbents, the sorbents show different particle size and degree of agglomeration. The average particle sizes are 400, 300, 200, and 500 nm for the $MgO/CaO/C$, $MgO/2CaO/C$, $MgO/4CaO/C$, and $MgO/8CaO/C$ sorbents, respectively. As shown in Fig. 5c, the particles of the $MgO/4CaO/C$ sorbent are not only smaller but also more evenly distributed and the agglomeration phenomenon of this sorbent is significantly reduced. Small particle size, evenly distributed structure, and low degree of agglomeration facilitate the adsorption of CO_2 . When the proportion of calcium oxide is further increased, the particle of the sorbent ($MgO/8CaO/C$ sorbent) becomes larger and a serious agglomeration occurs, as shown in Fig. 5d. For this

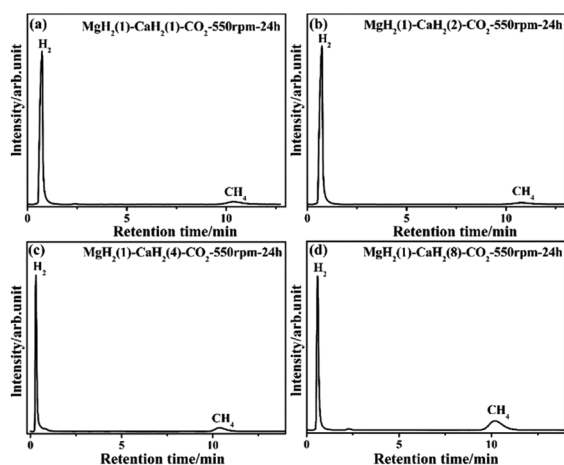


Fig. 2 GC profile of gas products for the ball milling reactions between the MgH_2/CaH_2 mixtures (with 1 : 1, 1 : 2, 1 : 4 and 1 : 8 mol mol⁻¹) and CO_2 at 550 rpm for 24 h.

Table 1 The yield and mole fraction of CH_4 and conversion of CO_2 for the ball milling reactions between the MgH_2/CaH_2 mixtures (with 1 : 1, 1 : 2, 1 : 4 and 1 : 8 mol mol⁻¹) and CO_2 at 550 rpm for 24 h

Reaction systems	Yield of CH_4 (%)	Mole fraction of CH_4 (%)	Conversion of CO_2 (%)
$MgH_2-CaH_2-CO_2$	14	22.3	100
$MgH_2-2CaH_2-CO_2$	18	24.8	100
$MgH_2-4CaH_2-CO_2$	30	32.5	100
$MgH_2-8CaH_2-CO_2$	16	24.2	100



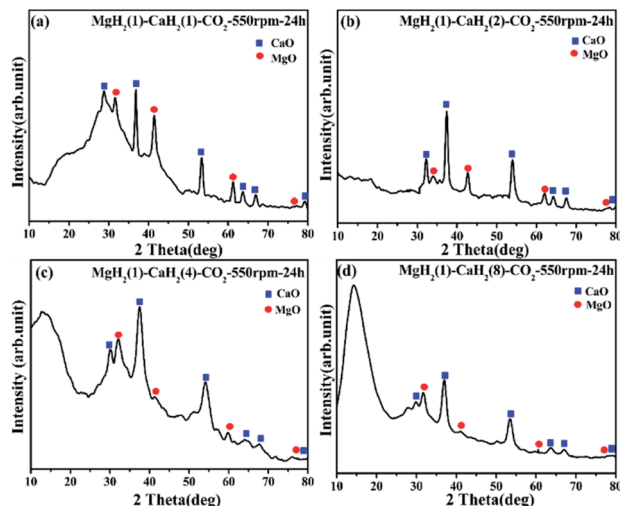


Fig. 4 XRD pattern of the solid products for the ball milling reactions between the $\text{MgH}_2/\text{CaH}_2$ mixtures (with (a) 1 : 1, (b) 1 : 2, (c) 1 : 4 and (d) 1 : 8 mol mol⁻¹) and CO_2 at 550 rpm for 24 h.

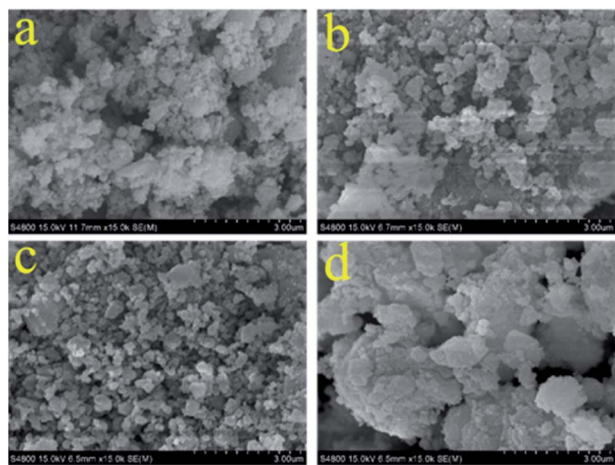


Fig. 5 SEM images of the (a) $\text{MgO}/\text{CaO}/\text{C}$; (b) $\text{MgO}/2\text{CaO}/\text{C}$; (c) $\text{MgO}/4\text{CaO}/\text{C}$; (d) $\text{MgO}/8\text{CaO}/\text{C}$ sorbents before carbonation/calcination cycles sorbents.

structure, blocking of the pores on the surface of the adsorbent and sintering phenomenon during the carbonation is easy to happen, which will affect the stability of the adsorption performance. For gas adsorption, in addition to the morphology, the specific surface area and pore volume of the sample also have a certain influence on the adsorption performance. As shown in Table 2, the specific surface area of the four sorbents is between 60.9 and 144.5 $\text{m}^2 \text{g}^{-1}$ and the BJH pore volume is between 0.1175 and 0.1942 $\text{cm}^3 \text{g}^{-1}$. It is noted that the $\text{MgO}/4\text{CaO}/\text{C}$ sorbent possesses a larger specific surface area and pore volume, which is favorable for the adsorption of CO_2 . The pore size distribution of all the adsorbent materials is shown Fig. S1.† We can see that the pore size distribution of the four samples is basically between 2 and 4 nm.

MgO , which has a high Tamm temperature, may play a role of skeleton support for CaO in the four synthetic sorbents,

Table 2 Summary of BET surface areas and BJH pore volumes for the sorbents

Sorbents	BET surface area [$\text{m}^2 \text{g}^{-1}$]	BJH pore volume [$\text{cm}^3 \text{g}^{-1}$]
$\text{MgO}/\text{CaO}/\text{C}$	60.9	0.1175
$\text{MgO}/2\text{CaO}/\text{C}$	85.5	0.1223
$\text{MgO}/4\text{CaO}/\text{C}$	116.8	0.1942
$\text{MgO}/8\text{CaO}/\text{C}$	144.5	0.1588

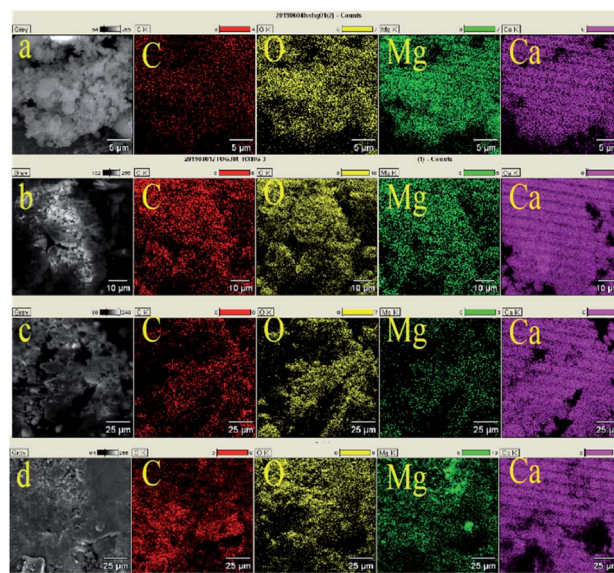


Fig. 6 SEM image and digital color EDX mapping images of carbon, oxygen, magnesium and calcium of (a) $\text{MgO}/\text{CaO}/\text{C}$; (b) $\text{MgO}/2\text{CaO}/\text{C}$; (c) $\text{MgO}/4\text{CaO}/\text{C}$; (d) $\text{MgO}/8\text{CaO}/\text{C}$ sorbents.

increasing its anti-sintering ability and improving cycle stability. The inert carbon in the sorbent, which has a large surface area and excellent heat transfer performance, may also reduce the sintering of CaO and promote the dispersion of CO_2 , which will result in the improvement of the CO_2 storage performance of the sample to some extent. The distribution of each element observed by EDX is shown in Fig. 6. We can see that the four elements of carbon, magnesium, oxygen, and calcium, are relatively uniform in each sample. It is expected that the uniformly distributed anti-sintered MgO and carbon particles effectively reduce the contact area between adjacent CaO particles, thereby minimizing the sintering phenomenon.

CO_2 capture properties of the MgO and carbon-doped CaO -based CO_2 sorbent

CO_2 isothermal adsorption properties of the four sorbents at 500, 650, and 750 $^\circ\text{C}$ were investigated and shown in Fig. 7. A large amount of adsorption occurs for all four samples in the initial period of adsorption, indicating that the initial adsorption rates of the four samples are fast and close. At 500 $^\circ\text{C}$, the $\text{MgO}/4\text{CaO}/\text{C}$ sorbent shows a better adsorption rate in the diffusion-controlled reaction stage. At 650 and 750 $^\circ\text{C}$, the



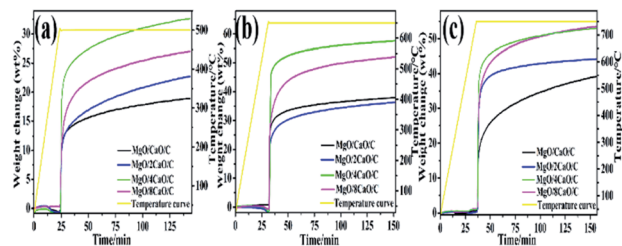


Fig. 7 CO₂ isothermal adsorption properties (in 100% CO₂) of the MgO/CaO/C, MgO/2CaO/C, MgO/4CaO/C and MgO/8CaO/C sorbents at different temperatures. (a) At 500 °C; (b) at 650 °C; (c) at 750 °C.

adsorption rate becomes poor in the diffusion control reaction stage, since the adsorption amount of each sample is basically saturated. However, as shown in Fig. 7a and b, among the four sorbents the MgO/4CaO/C sorbent exhibits the highest adsorption capacity at 500 and 650 °C (reaching 35 wt% and 55 wt%, respectively). As the adsorption temperature is increased from 500 to 650 °C, the adsorption amount of each sample is significantly improved. At 750 °C, the adsorption amount of the MgO/CaO/C, MgO/2CaO/C, and MgO/8CaO/C sorbents is further improved. The adsorption at 650 °C is more suitable in view of the reaction temperature and energy consumption.

To examine the stability of four adsorbents for adsorbing CO₂, we performed 30 carbonation/calcination cycles. Fig. 8 shows the cyclic performance of four adsorbents. The carbonation was performed at 650 °C for 2 h in 100% CO₂, while the calcination was implemented at 800 °C for 15 min in 100% Ar. Fig. 9 summarizes the adsorption capacity after each cycle of carbonation for the four sorbents. We can see from Fig. 8a and b that the initial adsorption amount of the MgO/CaO/C and MgO/2CaO/C samples is 37.9 and 37.8 wt%, respectively. There is a slight increase in the amount of adsorption in the next two

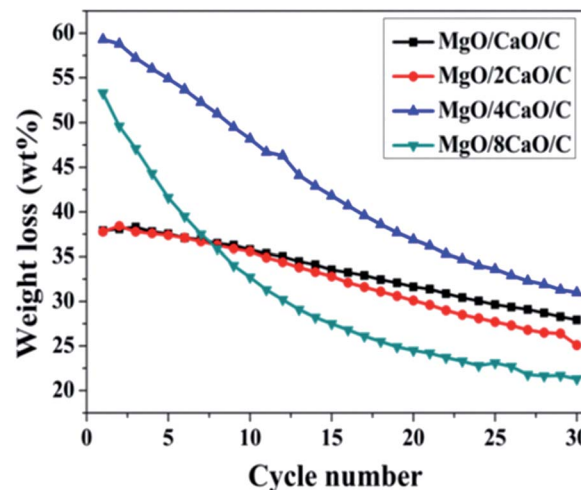


Fig. 9 CO₂ uptake as a function of cycle number.

cycles, which is a result of self-activation,²³ as reported in the literature. Then the amount of adsorption gradually decreases in the remaining cycles. It is well known that CaO cannot maintain CO₂ adsorption during the carbonation/calcination cycle, which is mainly due to the thermal sintering of CaO. Powder will gradually become denser, and the average particle size will increase, as thermal energy is applied to it, which results in the sintering of the sorbent.¹² Due to the different methanation degree of CO₂, the amount of amorphous carbon in the samples is 0.0056–0.007 mol. Carbon is one of the important components of Mg/Ca/C sorbents and may reduce CaO sintering and promote CO₂ adsorption. The adsorption amount of MgO/CaO/C is decreased to 27.9 wt% after 30 cycles, being deactivated by 10 wt%. Similarly, the MgO/2CaO/C adsorption amount is decreased to 25.1 wt%, being deactivated by 12.7 wt%. The adsorption capacity is relatively stable, indicating that the incorporation of MgO does play a role in the anti-sintering effect and can improve the stability of CaO adsorption performance. Due to the large amount of MgO in the two samples of MgO/CaO/C and MgO/2CaO/C, the initial adsorption amount of the two samples is relatively low. Fig. 8c and d shows the results of adsorption of MgO/4CaO/C and MgO/8CaO/C during 30 cycles, respectively. We can see that the initial adsorption amount of the MgO/4CaO/C and MgO/8CaO/C sorbent is relatively high, being 59.3 and 53.3 wt%, respectively. Although the initial adsorption amount is significantly increased due to the increase of CaO content in the two samples of MgO/4CaO/C and MgO/8CaO/C, the sintering resistance of the sample is lowered, and the cycle stability is also reduced due to the decrease of the content of MgO. After 30 cycles, the adsorption amount of MgO/4CaO/C and MgO/8CaO/C was 31 and 21.3 wt%, being decreased by 28.3 and 32 wt%, respectively. Since the particle of MgO/4CaO/C is uniformly dispersed, and there is no agglomeration phenomenon (Fig. 5), the initial adsorption amount of MgO/4CaO/C is higher than that of MgO/8CaO/C. At the same time, the content of MgO in MgO/4CaO/C is higher than that of MgO/8CaO/C, so the cycle stability is

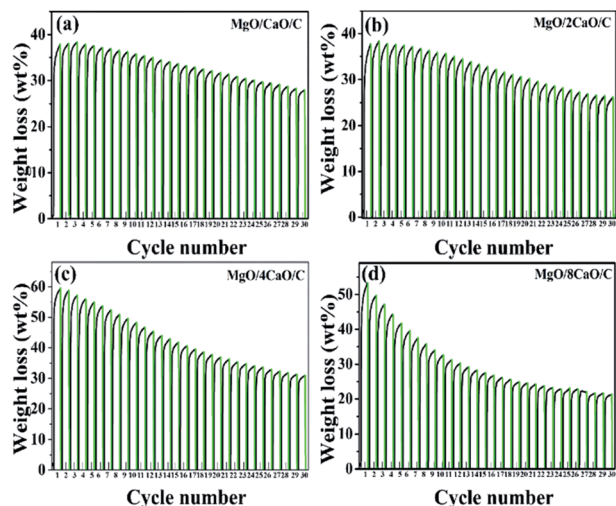


Fig. 8 TGA data showing the CO₂ adsorption–desorption capacity over 30 cycles of the (a) MgO/CaO/C; (b) MgO/2CaO/C; (c) MgO/4CaO/C; (d) MgO/8CaO/C sorbents.

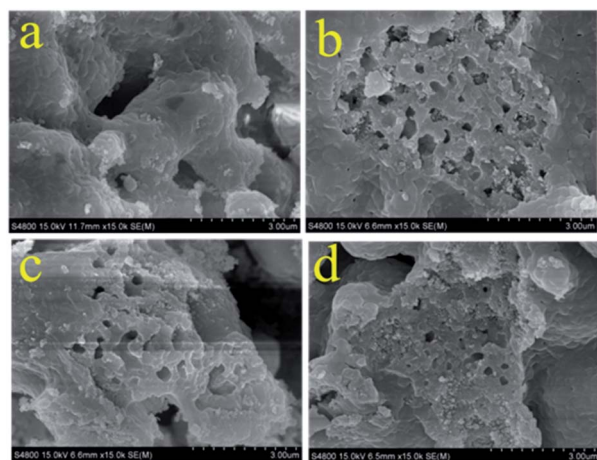


Fig. 10 SEM images of the (a) MgO/CaO/C; (b) MgO/2CaO/C; (c) MgO/4CaO/C; (d) MgO/8CaO/C sorbents after 30 carbonation/calcination cycles.

better. From the data in Fig. 9, we can see that when the MgO content is high, it is favorable for the stability of cycle, and when the CaO content is high, it is advantageous for the increase of the adsorption amount. When MgO and CaO are mixed with a proper amount, they can show a better adsorption capacity. It is not necessary that the higher the CaO ratio, the better the adsorption capacity.² When CaO is too much and MgO is too few, MgO cannot be uniformly dispersed in CaO, and it cannot play a good role in supporting the framework, resulting in serious agglomeration of CaO, which affects its adsorption amount. Overall, the adsorption performance of the MgO/4CaO/C sorbent is better than that of the other three sorbents because it exhibits higher initial adsorption capacity and better cycle stability. As mentioned above, the synergistic effects of MgO and carbon results in the improvement of CaO adsorption performance in MgO/4CaO/C sorbent.

The morphology change of each sample after adsorption was examined by SEM (Fig. 10). The morphology of the samples changes significantly after 30 carbonation/calcination cycles, compared with that before cycles (Fig. 5). It can be observed from Fig. 10a and b, that both the MgO/CaO/C and MgO/2CaO/C sorbents sinter to some degree, but there are still distinct and relatively much pore structures in the sorbents. Therefore, their adsorption performance is relatively stable. As exhibited in Fig. 10c and d, the MgO/4CaO/C and MgO/8CaO/C sorbents show more obvious sintering phenomena. There are fewer and smaller pore structures in the MgO/4CaO/C and MgO/8CaO/C sorbents after cycles.

Thereby, the adsorption stability of the MgO/CaO/C and MgO/2CaO/C sorbents is better than that of the MgO/4CaO/C and MgO/8CaO/C sorbents. Fig. 11 shows the XRD patterns of four samples after 30 cycles of carbonation/calcination. Characteristic peaks of CaO and MgO and weak peaks of CaCO₃ and MgCO₃ can be observed from Fig. 11a–d. During the carbonation process, most of CaO in the sorbents is carbonated to CaCO₃. However, calcination does not completely decarburize the sample due to sintering. Part of the generated CaCO₃ could

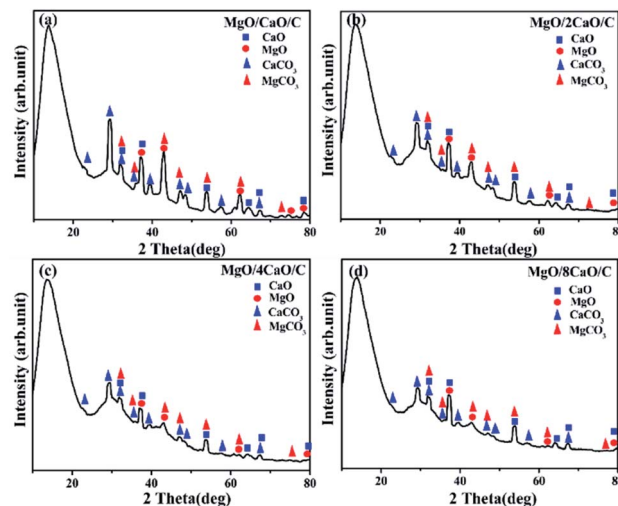


Fig. 11 XRD patterns of the (a) MgO/CaO/C; (b) MgO/2CaO/C; (c) MgO/4CaO/C; (d) MgO/8CaO/C sorbents after 30 carbonation/calcination cycles.

not be fully calcined and returned to CaO, which had an impact on the subsequent cycle performance. This is also the reason that the adsorption performance is degraded in addition to sintering.

Table 3 compares the CO₂ adsorption properties of MgO/CaO adsorbents prepared by various synthetic methods. The performance of the four samples in this experiment is also shown in Table 3. It can be seen that the MgO/CaO/C sample shows higher adsorption stability (the average deactivation rate after 30 cycles is 0.88) and lower initial adsorption amount (only 37.9 wt%). The MgO/4CaO/C sample exhibits higher initial adsorption capacity (59.3 wt%) and good adsorption stability (the average deactivation rate after 30 cycles is 1.6%). The initial adsorption amounts of the MgO/CaO adsorbents prepared by Zhu²⁴ and Sayyah²⁵ using the ball milling method were 65 wt% and 49 wt%, respectively; the average deactivation rates were 0.42% and 0.37%, respectively. Kurlov reported that, for the MgO/CaO adsorbent synthesized by wet ball milling, the initial adsorption amount was 64 wt% and the average deactivation rate was about 1.77%.²⁶ The initial adsorption capacity of MgO/4CaO/C is higher than that reported by Sayyah,²⁵ and the cycle stability is better than that reported by Kurlov.²⁶ Moreover, the initial adsorption amount of the MgO/4CaO/C sorbent is higher than that of the natural MgO/CaO by 45 wt%.⁷ Daud,²⁰ Park,⁸ and López²⁷ reported that the initial adsorption amounts of MgO/CaO adsorbents synthesized by co-precipitation method were 39–58 wt%, respectively, which is lower than that of the MgO/4CaO/C sorbent. In addition, the initial adsorption amount of MgO/4CaO/C (59.3 wt%) was higher than that of the synthetic adsorbent reported by Phromprasit (25.9 wt%),¹⁹ Pi (52 wt%),²⁸ Miranda-Pizarro (46 wt%),²⁹ Park (46 wt%),⁸ Yang (45 wt%),⁷ Ping (32.6 wt%)²² and Lan (45 wt%).³⁰ At the same time, for the capacity of the MgO/4CaO/C sorbent, there is comparability with that of the adsorbent reported by Naeem (62 wt%),¹ Yan (58 wt%)³¹ and López (58 wt%).²⁷ The adsorption



Table 3 Various CaO-based CO₂ sorbents: comparison of synthesis methods, testing conditions, CO₂ uptakes, and activity loss

Adsorbent	Synthesis method	Temperature [°C]		Number of cycles	CO ₂ uptake at first/last cycle [wt%]	Average activity loss per cycle [%]	Ref.
		Carbonation	Calcination				
MgO/CaO/C	Ball-milling	650	800	30	37.9–27.9	0.88	This work
MgO/2CaO/C	Ball-milling	650	800	30	37.8–25.1	1.12	This work
MgO/4CaO/C	Ball-milling	650	800	30	59.3–31	1.6	This work
MgO/8CaO/C	Ball-milling	650	800	30	53.3–21.3	2.01	This work
MgO/CaO	Ball milling	680	780	100	65–38	0.42	24
MgO/CaO	Ball milling	650	900	50	49–40	0.37	25
MgO/CaO	Wet ball-milling	650	900	30	64–30	1.77	26
MgO/CaO	Natural CaO–MgO	650	850	50	45–26	0.84	7
MgO/CaO	Co-precipitation method	650	800	30	39–42	+0.26	20
MgO/CaO	Co-precipitation method	700	700	60	46–43.5	0.1	8
MgO/CaO	Co-precipitation method	650	900	40	58–30	1.2	27
MgO/CaO	CaO hydration method	600	850	10	25.9–25.2	0.27	19
MgO/CaO	CaO hydration method	700	850	20	58–52	0.52	31
MgO/CaO	Extrusion and spheronization, method	650	900	25	52–23	2.23	28
MgO/CaO	Pretreated with diluted acetic acid	650	900	20	46–38	0.87	29
MgO/CaO	Re-crystallization	650	900	10	66.9–47.1	3	32
MgO/CaO	Adsorption phase reaction technique	700	730	30	32.6–30	0.27	22
MgO/CaO	Sol–gel method	700	850	20	45–34	1.22	30
MgO/CaO	Pechini method	650	900	10	62–44.9	1.71	1

stability of the MgO/4CaO/C sorbent is better than that reported by Pi (average inactivation rate 2.23%),²⁸ Broda (average inactivation rate 3%),³² Naeem (average inactivation rate 1.71%),¹ and Kurlov (average inactivation rate 1.77%).²⁶ Compared with the MgO/CaO adsorbents prepared by other methods, the MgO/4CaO/C sorbent synthesized in this experiment shows higher initial adsorption amount or comparable cycle stability. Moreover, the method to prepare the MgO/4CaO/C sorbent requires simple steps, is easy to operate, does not need various solvents, does not cause secondary pollution, and is suitable for mass production.

Conclusions

Mechanochemical reduction of CO₂ by MgH₂/CaH₂ mixture with 1 : 1, 1 : 2, 1 : 4 and 1 : 8 mol mol^{−1} was first performed, by which we achieve selective methanation of CO₂ and acquire effective CaO-based CO₂ sorbents, simultaneously. In these reactions, CO₂ is completely converted and CH₄ is the sole hydrocarbon product in the gas phase. The selectivity of methanation is near 100% and the yield of CH₄ reaches 30%. In addition, the solid products, which are composed of MgO, CaO, and Carbon, are novel, highly effective CaO-based CO₂ sorbents. Among the prepared sorbents, the MgO/4CaO/C sorbent shows high initial adsorption amount of 59.3 wt% and low average activity loss of 1.6% after 30 cycles. The improvement of CaO adsorption performance in MgO/4CaO/C sorbent results from the synergistic effects of MgO and carbon. This work provides

a novel, well-scalable, and sustainable approach to prepare an efficient inert additive-included CaO-based CO₂ sorbent and selectively convert CO₂ to CH₄ at the same time.

Conflicts of interest

There are no conflicts to declare.

Acknowledgements

This study is supported by the National Natural Science Foundation of China (No. 21671169 and 21573192) and the Foundation from the Priority Academic Program Development of Jiangsu Higher Education Institutions.

Notes and references

- 1 M. A. Naeem, A. Armutlulu, Q. Imtiaz and C. R. Müller, *ChemPhysChem*, 2017, **18**, 3280–3285.
- 2 Q. F. Shi, J. Wu and S. L. Mu, *J. Electroanal. Chem.*, 2018, **820**, 1–8.
- 3 K. Kim, J. W. Han, K. S. Lee and W. B. Lee, *Phys. Chem. Chem. Phys.*, 2014, **16**, 24818–24823.
- 4 A. Hafizi, M. R. Rahimpour and S. Hassanajili, *Appl. Energy*, 2016, **169**, 629–641.
- 5 J. M. Valverde, P. E. Sanchez-Jimenez, A. Perejon and L. A. Perez-Maqueda, *Phys. Chem. Chem. Phys.*, 2013, **15**, 11775–11793.



- 6 S. Tian, J. Jiang, F. Yan, K. Li and X. Chen, *Environ. Sci. Technol.*, 2015, **49**, 7464–7472.
- 7 X. Yang, L. Zhao, S. Yang and Y. Xiao, *Asia-Pac. J. Chem. Eng.*, 2013, **8**, 906–915.
- 8 J. Park and K. B. Yi, *Int. J. Hydrogen Energy*, 2012, **37**, 95–102.
- 9 Q. Zhu, S. Zeng and Y. Yu, *Environ. Sci. Technol.*, 2016, **51**, 552–559.
- 10 K. Wang, X. Guo, P. Zhao, L. Zhang and C. Zheng, *Chem. Eng. J.*, 2011, **173**, 158–163.
- 11 M. Broda, A. M. Kierzkowska and C. R. Müller, *ChemSusChem*, 2012, **5**, 411–418.
- 12 P. H. Chang, Y. P. Chang, S. Y. Chen, C. T. Yu and Y. P. Chyou, *ChemSusChem*, 2011, **4**, 1844–1851.
- 13 H. Ping and S. Wu, *ACS Sustainable Chem. Eng.*, 2016, **4**, 2047–2055.
- 14 H. Chen, C. Zhao and W. Yu, *Appl. Energy*, 2013, **112**, 67–74.
- 15 R. Sun, Y. Li, H. Liu, S. Wu and C. Lu, *Appl. Energy*, 2012, **89**, 368–373.
- 16 F. Yan, J. Jiang, K. Li, S. Tian, Z. Liu and J. Shi, *ACS Sustainable Chem. Eng.*, 2016, **4**, 7004–7012.
- 17 X. Zhang, Z. Li, Y. Peng, W. Su, X. Sun and J. Li, *Chem. Eng. J.*, 2014, **243**, 297–304.
- 18 W. Peng, Z. Xu, C. Luo and H. Zhao, *Environ. Sci. Technol.*, 2015, **49**, 8237–8245.
- 19 J. Phromprasit, J. Powell and S. Assabumrungrat, *Chem. Eng. J.*, 2016, **284**, 1212–1223.
- 20 F. D. M. Daud, K. Vignesh, S. Sreekantan and A. R. Mohamed, *New J. Chem.*, 2016, **40**, 231–237.
- 21 L. Huang, Q. Zheng, B. Louis and Q. Wang, *Energy Technol.*, 2018, **6**, 2469–2478.
- 22 H. Ping, Y. Wang and S. Wu, *RSC Adv.*, 2016, **6**, 41239–41246.
- 23 P. Lan and S. Wu, *Fuel*, 2015, **143**, 9–15.
- 24 Q. Zhu, S. Zeng and Y. Yu, *Environ. Sci. Technol.*, 2016, **51**, 552–559.
- 25 M. Sayyah, Y. Lu, R. I. Masel and K. S. Suslick, *ChemSusChem*, 2013, **6**, 193–198.
- 26 A. Kurlov, M. Broda, D. Hosseini, S. J. Mitchell, J. Pérez-Ramírez and C. R. Müller, *ChemSusChem*, 2016, **9**, 2380–2390.
- 27 J. M. López, G. Grasa and R. Murillo, *Chem. Eng. J.*, 2018, **350**, 559–572.
- 28 S. Pi, Z. Zhang, D. He, C. Qin and J. Ran, *Energy Fuels*, 2019, **33**, 2381–2389.
- 29 J. Miranda-Pizarro, A. Perejón, J. M. Valverde, L. A. Pérez-Maqueda and P. E. Sánchez-Jiménez, *Fuel*, 2017, **196**, 497–507.
- 30 P. Lan and S. Wu, *Chem. Eng. Technol.*, 2014, **37**, 580–586.
- 31 X. Yan, Y. Li, X. Ma, J. Zhao, Z. Wang and H. Liu, *New J. Chem.*, 2019, **43**, 5116–5125.
- 32 M. Broda, A. M. Kierzkowska and C. R. Müller, *Adv. Funct. Mater.*, 2014, **24**, 5753–5761.
- 33 H. Lu, X. Yang, G. Gao, J. Wang, C. Han, X. Liang, C. Li, Y. Li, W. Zhang and X. Chen, *Fuel*, 2016, **183**, 335–344.
- 34 C. Liang, Z. Ye, D. Dong, S. Zhang, Q. Liu, G. Chen, C. Li, Y. Wang and X. Hu, *Fuel*, 2019, **254**, 115654.
- 35 M. L. Grasso, J. Puszkiel, L. F. Albanesi, M. Dornheim, C. Pistidda and F. C. Gennari, *Phys. Chem. Chem. Phys.*, 2019, **21**, 19825–19834.
- 36 B. X. Dong, J. Zhao, L. Z. Wang, Y. L. Teng, W. L. Liu and L. Wang, *Appl. Energy*, 2017, **204**, 741–748.

